Hardening prediction of diverse materials using the Digital Image Correlation technique

Julen Agirre[a, 1], Joseba Mendiguren[a], Lander Galdos[a], Eneko Saenz de Argandoña[a]

a) Department of Mechanical and Industrial Production, Mondragon Unibertsitatea, Loramendi 4, Mondragon 20500, Gipuzkoa, Spain

1) Corresponding author: jagirreb@mondragon.edu, +34687001422

Abstract. In recent years, due to the introduction of higher resistance materials in the automotive sector, sheet metal-forming tool-makers have been forced to deal with more challenging process designs. Therefore, the optimisation of the manufacturing process has become a key factor in obtaining a part which fits the required tolerances, and the Finite Element Method (FEM) is the most widely used technique to speed up that optimisation time. However, to obtain a numerical result as close as possible to those of industrial conditions, the FEM software inputs must be highly accurate. The present work is focused on the hardening extension of the currently available reduced-formability materials, as it is a key factor in the correct prediction of the stress state and hence, of the springback during a sheet metal-forming process. The objective in this work was the selection of the most appropriate hardening model to extend the flow curve beyond the necking limit for a wide variety of material families currently utilised in the industrial environment. To carry out that analysis, a Digital Image Correlation (DIC) technique was utilised during conventional tensile tests to extend the experimental flow curves of the analysed materials. Commonly used hardening models were fitted to the experimental tensile flow curves with the aim of selecting the model that best predicts the hardening behaviour of each analysed material family. The results showed that the DIC technique was valid for the extension of the hardening curve of the analysed materials and for the final selection of the most suitable hardening model for each analysed material family.

Keywords. Hardening model; DIC; Isotropic hardening; Metal forming

1. INTRODUCTION

New CO_2 emission regulations together with increased safety standards in the automotive sector have forced manufacturers to dedicate considerable time and resources reducing the weight of car body components. With this aim, design optimisation and further studies of new materials have been carried out in recent decades. As González Palencia et al. (2012) stated, new materials such as aluminium, magnesium or carbon fibre-reinforced composites have been incorporated into high-end cars, and steel makers have developed stronger steel grades to reduce the thickness of components and therefore car weight (advanced high-strength steels, or AHSS). Examples of these new steels are DP1000 and MS1200 whose formability and hardening behaviour was analysed by Silvestre et al. (2015), or the third-generation steels discussed by Askari-paykani et al. (2016). These materials have contributed towards the cost reduction of first and second generation steels but still maintain a combination of high tensile strength and a competitive elongation capacity.

The introduction of AHSS to the automotive environment has resulted in important manufacturing challenges, as compared to conventional steels, they allow reduced elongation levels and lead to higher springback (elastic recovery after forming), forming forces and wear. Panich et al. (2016) investigated the ductile damage initiation and fracture of AHSS by tensile testing diverse specimen geometries to better understand this phenomenon. As an example, a typical drawing steel (such as, DC04 or DX56) has a yield strength of around 100-200 MPa and an elongation of 35–40% (Suttner and Merklein, 2017). Silvestre et al. (2015) compared the hardening behaviour of different steel families and determined that a martensitic steel (MS1200, MS1400) has a yield strength of around 1200–1400 MPa, but has a limited elongation to rupture of around 2–4%. Even when the formability of these materials is high enough to obtain a sound component, the high level of stresses they reach results in high springback phenomena. Gil et al. (2016) worked on the springback prediction of both mild steels and high strength steels by studying the influence of the pressure dependent coefficient of friction in deep drawing operations.

To overcome the abovementioned manufacturing limitations, and to optimise tools and processes in sheet metal-forming operations, toolmakers make use of Finite Element Method (FEM) software to obtain virtual predictions of the process. With this technique, the high springback levels, drawing efforts and tendency to crack present in AHSS can be taken into account in the process design. Finite element simulation validation was carried out by Ul Hassan et

al. (2016) to determine accurate springback predictions in deep drawing using pre-strained based multiple cyclic hardening curves. Lee et al. (2015) analysed the influence of material and friction models for springback and punch load predictions by utilizing FEM, and finite element simulation was employed by Teixeira et al. (2006) for the prediction of ductile fracture in sheet metal forming processes. However, both the literature and experience have demonstrated that the accuracy of FEM is highly dependent on the tribological and material constitutive models entered in the software.

Focusing on the material model, different phenomena have to be taken into account, for example elasticity, yielding, hardening and forming limit definition. Mendiguren et al. (2015a) characterized the elastic behaviour of the TRIP700 steel using loading-unloading tests. Neto et al. (2017) experimentally and numerically compared the yielding of a mild steel and a dual-phase steel to analyse the influence of boundary conditions on the prediction of springback and wrinkling in sheet metal forming. The Bauschinger effect in dual-phase steels at strain levels close to the ones observed in automotive stamping was investigated by Weiss et al. (2015) so as to characterize kinematic hardening for numerical simulation and Peng et al. (2017) worked on the plastic forming limit of sheet metals by employing various failure criteria. Among the aforementioned material properties, hardening is what defines the final stress state of the material after a certain elongation, and this has a significant impact on the springback the material will suffer, the forming forces during the process and the forming limits of the material. To analyse the elastic recovery the material suffers after forming, Oliveira et al. (2005) studied the influence of work hardening model parameters on springback prediction in mild and dual-phase steels. Hora (2006) compared two of the most widely used pure isotropic hardening models in order to analyse their influence on the hardening behaviour and the forming limit curve of a material.

Material hardening can be modelled as isotropic, kinematic or mixed hardening. Butuc et al. (2011) analysed the formability of sheet metals utilizing various isotropic and kinematic hardening models. Mendiguren et al. (2015b) developed a kinematic hardening effect graph to estimate the influence of kinematic hardening on the model employed in numerical sheet metal forming simulations, avoiding the cost- and time-consuming material characterization tests. As for mixed hardening, Yu and Chen (2017) proposed an isotropic-kinematic model taking into account the transformation-induced plasticity effect for TRIP steels. New theories are now being introduced, such as distortional hardening presented by Manopulo et al. (2015), but they are still at the research stage. However,

the isotropic models remain the most widely used, where the strain hardening is taken into account and the yield stress evolution is represented depending on the plastic strain.

The most commonly used characterisation technique to obtain the stress-strain curve of a material is the tensile test, in which a specimen is loaded in a uniaxial state. The major limitation of this characterisation technique when applied to sheet metal-forming operations is the reduced elongations which can result (Shirgaokar et al. (2008)). In metal-forming processes such as deep drawing or stamping operations, the metal sheet is deformed in such a way that the loading strain path can differ from that of the tensile test. In a tensile test the specimen is loaded in a uniaxial stress state, while in metal-forming processes, this stress state can vary from shear to biaxial stresses, postponing the onset of necking and thereby obtaining greater elongations than those of conventional tensile tests (Suttner and Merklein, 2016).

For this reason, different experimental techniques are used to extend the tensile test flow curve of a material to higher strain values, for example, the bulge test and shear test. The bulge test is carried out to determine the behaviour of the material under biaxial stretching. Mulder et al. (2015) worked on the precise measurement of flow curves employing the bulge test by adding optical measuring systems. In this way, they were able to obtain more detailed deformation values at high strains compared to those obtained by typical mechanical measuring systems. However, as stated in Kuwabara (2007), the main drawbacks to this technique include its high economic cost and technical complexity, apart from the need for special equipment. Other techniques used to extend the stress-strain curve beyond the tensile necking limit are the biaxial tension and biaxial compression tests. Merklein and Biasutti (2013) developed a biaxial machine for sheet metal hardening characterization and Liu et al. (2015) carried out in-plane biaxial tensile tests using cruciform specimens to identify sheet metal hardening behaviour for large strains. As for biaxial compression, Zillmann et al. (2014) performed this test to determine the hardening behaviour at high strain levels and the tension-compression asymmetry in materials that present a strength-differential (Bauschinger effect). Nevertheless, as in the case of the bulge test, these two techniques are expensive, because of the complex shapes of the specimens and a biaxial machine is needed (Kuwabara (2007)). Nolan and McGarry (2016) also found that, as the tension and compression tests are in a biaxial load condition, proper assumptions have to be made for the correct conversion to uniaxial values. An additional disadvantage in the case of

the biaxial compression test is that it presents difficulties in obtaining accurate flow curves, due to the friction between the specimen and the tool (Kuwabara (2007)).

Shear and torsion tests are the other two techniques used to obtain flow curves up to greater elongation levels. Yin et al. (2014) investigated experimentally and numerically diverse shear test configurations for sheet metal characterization and in 2015 carried out a grooved in-plane torsion test for the investigation of shear fracture and hardening at high elongations. The drawbacks however are that the specimens are complex, and the tests are expensive and time-consuming. Yin et al. (2014) also acknowledged that the results obtained from these tests are not directly comparable to uniaxial tensile test values.

Finally, an increasing practice used to extend typical stress-strain curves beyond the necking limit is to use digital image correlation (DIC) techniques. As an example, Gerbig et al. (2016) determined constitutive parameters in the necking of tensile specimens by coupling digital image correlation and finite element analysis. The mentioned DIC techniques are capable of acquiring accurate 2D and 3D images by means of artificial vision. Consequently, by registering and tracking those images it is possible to obtain accurate material data, such as deformation, displacement and strain.

In the past decade, DIC techniques have been applied in a variety of analyses in order to obtain advanced material characterisations. Sutton et al. (2009) introduced the basic concepts, theory and applications of digital image correlation for shape, motion and deformation measurements. Merklein et al. (2006) utilised DIC techniques to measure tensile test specimen deformations to determine the thermo-mechanical characteristics of an ultra-high strength steel (UHSS), and Holmberg et al. (2004) evaluated the forming limit of sheet metals by using DIC in tensile tests. DIC techniques have also been used to identify the plastic behaviour of a material by inverse modelling simulation and the virtual fields method. As an example, Grédiac and Pierron (2006) applied the virtual fields method to the identification of elasto-plastic constitutive parameters. Avril et al. (2008) presented an overview of mechanical parameter identification methods based on full-field measurements, and Rossi et al. (2013) made an attempt to characterise the plastic behaviour of aluminium alloys at high plastic strain values by using the virtual fields method. Many of the works published regarding the identification of post-hardening material behaviour have been based on the inverse modelling simulation. Eller et al. (2016), for instance, determined the strain hardening

parameter of tailor hardened boron steel at high strain levels utilizing inverse FEM optimization and strain field matching. Coppieters et al. (2011) compared the internal and external work in the necking zone of a sheet metal to identify post-necking hardening.

Although these techniques are capable of extending the flow curve of a material beyond the tensile necking point, in an industrial sheet metal-forming process even greater strain levels can be obtained (Larour, 2010). To simulate these industrial processes, the simulation software needs to have information about the hardening of the material at all the strain stages, that is to say, it needs to know the stress level which corresponds to each strain level during the whole process. Therefore, to define the flow curve of a material to strain levels up to 100% or more, a series of mathematical models known as hardening models are used.

Many examples of the use of hardening models in the extension of the hardening curve beyond the necking point have been found in the literature. Larour (2010) employed many classical pure isotropic hardening models to analyse the influence of plastic strain in automotive sheet steels and Saboori et al. (2014) used two of the most well-known hardening models (*Hollomon* and *Swift*) to extend the bulge test stress-strain curve of various aerospace alloys such as IN 718 and SS 321. A particular DIC method was utilised by Coppieters and Kuwabara (2014) to identify the post-necking strain hardening of ductile sheet metals and a pure titanium sheet, and then they were compared to different hardening model predictions (*Swift* and *Voce*). Zhang et al. (2015) analysed the hardening of two different morphologies of martensite in a dual-phase steel by using two hardening models (*Hollomon* and *Ludwik*). Another example is that of Wang et al. (2016), in which the approximation of the hardening of a dual-phase steel sheet was modelled with a different classical hardening model (*Swift-Hockett*/*Sherby*) to then simulate and predict the forming and springback of a part during a test. Nevertheless, material engineers and researchers always have to face the problem of having to select one model without knowing whether it is the optimum one for that specific material. The incorrect selection of a hardening model could lead to the underestimation or overestimation of the stress state, with all the consequences that ensue regarding force and springback levels.

The studies presented thus far have analysed the hardening behaviour of different materials by means of hardening models; nevertheless, these works have focussed on fitting the materials with no more than two hardening models. Taking into account that there are more analytical models which follow different hardening paths, it is

possible that the models utilised in these works were not the optimum ones. Consequently, a more detailed study needs to be carried out in which a wider variety of materials is fitted by a greater number of hardening models. Using this approach, the most suitable hardening model for each material can be selected.

The main objective of this work therefore is to determine the most optimum hardening model for each material family. To characterise the hardening behaviour of a material beyond the necking point, a DIC technique was employed to experimentally extend the flow curve obtained from a conventional tensile test. Once the experimental hardening behaviour of the material was known, various hardening models were fitted and compared to the extended experimental curve. Finally, the ability of each model to represent the real behaviour of the material was determined. This procedure was carried out with a variety of material families with the objective of selecting the hardening model which best fits each of the analysed material families.

2. METHODOLOGY

The DIC technique is applied in the accurate measurement of a wide variety of parameters via artificial vision, and it is utilised in diverse scientific and engineering areas. In this work, DIC was used to extend the flow curve of a material during a conventional tensile test beyond the necking point to higher strain values. The methodology explained below has been applied in a wide variety of materials which are currently used in many industrial applications (Figure 1).

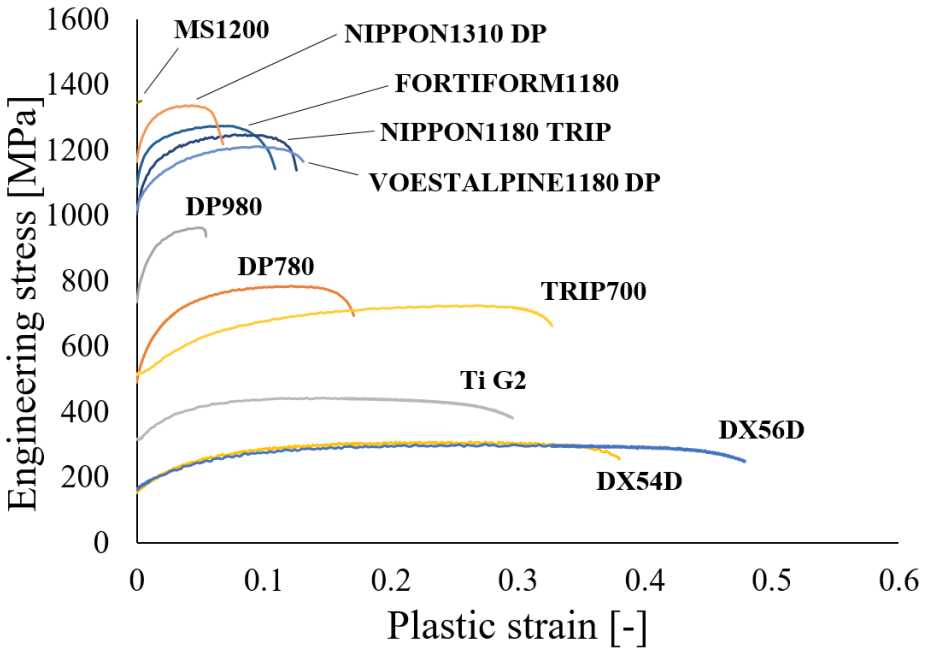

Figure 1: Technical stress–plastic strain curves of the analysed materials

The DIC-based system employed to carry out the required measurements in this work was the GOM Aramis 5M®. This system is a non-contact measuring facility composed of a series of highly precise stereo-vision devices, commonly used to measure and determine diverse material parameters. One of the main advantages of this system is its high integration capacity into existing test environments via external triggering and analogue data acquisition (GOM, 2016).

In the present work, this system was utilised to obtain material parameters from a conventional tensile test. This artificial vision is capable of measuring the strain distribution of a testing specimen, and it is also able to capture the force signal enabling the synchronisation of both the force and the strain data (GOM, 2014). In the present work, a first measuring strategy was followed to obtain pre-necking tensile values. In this step, a large surface area was

defined along the length of the sample by means of artificial vision (Figure 2). Measuring the strain distribution of that selected area and taking into account the load values provided by the tensile machine (50 kN Instron/Zwick 3369), the average tensile values were acquired which showed good agreement with those obtained in a standard tensile test without DIC (GOM, 2014). In this paper, this first measuring stage will be called the Before-Necking Measurement (BNM).

A second measuring strategy was followed to acquire material properties after the necking limit. The theory behind this strategy considers that if the localised necking zone of the specimen still follows a homogeneous strain distribution, the loading condition can be assumed as uniaxial, obtaining stable local values (GOM, 2014). It is understood that in the necking area of the specimen the homogeneity is lessened, but considering a small area in the necking zone, values close to the homogenous ones can be acquired during part of the necking (GOM, 2014) (Figure 2). In calculating the average values of that localised area, mechanical properties can be obtained beyond the necking point up to a point close to the fracture of the specimen. Therefore, by using this technique, the true stress-true strain curve of the material can be extended to greater strains. The major advantage of this procedure is its simplicity, since from a standard tensile test, by just adding external artificial vision devices, larger strain values can be achieved. The drawback of this strategy however, is the fact that in the final stages of the test, close to the fracture, the final values of the curve have to be considered invalid because the strain distribution loses its homogeneity. This method is also highly dependent on the post-necking behaviour of the material. If the necking and fracture points are close to each other, this technique does not offer much information. For the purposes of this article, this second measuring stage is called the After-Necking Measurement (ANM).

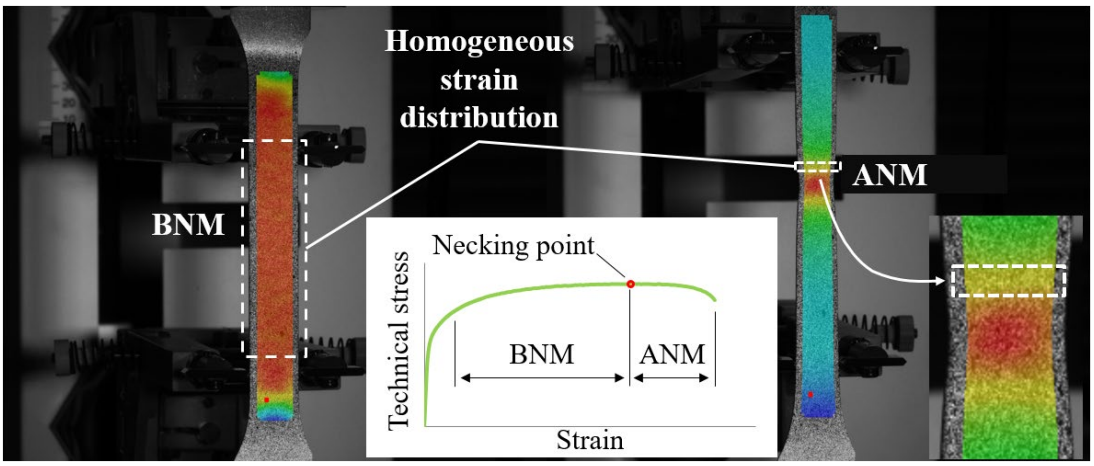

Figure 2: Homogeneous strain distribution of a specimen during different tensile stages

The technical specifications entered in the GOM Aramis 5M® system to carry out the measurements are as follows. As a compromise between accuracy and computation time, the facet size utilised in the measurements was 19 x 19 pixels, and the facet step was 15 pixels. The frame rates employed to obtain the BNM and the ANM values were 0.5 and 15 frames per second, respectively (the rate of 15 frames per second was also used for the elastic part of the BNM).

In order to ensure that the values obtained from the tests were trustworthy, three tensile tests were performed for each material; however, just one representative curve was utilised for the study as the results showed good repeatability. The strain-extending capacity of both the BNM and ANM procedures is presented in Figure 3.

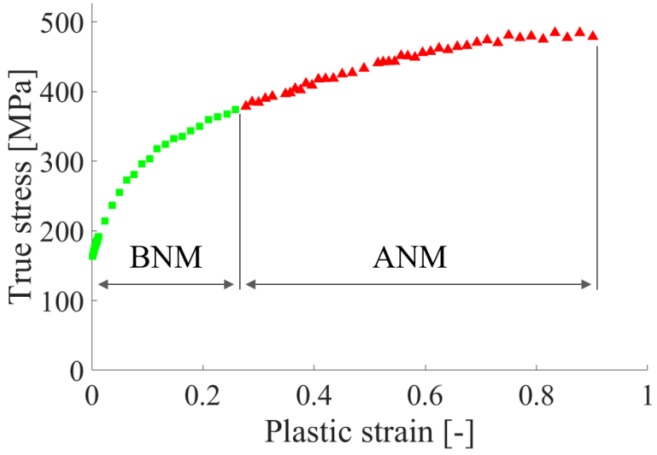

Figure 3: BNM and ANM hardening curves of a DX56D mild steel

The tool utilised to calculate the fittings of the aforementioned hardening models was the numerical computing software Matlab®. First, all hardening models were fitted to the last third of the BNM experimental hardening curve by the least squares method (Figure 4). The reason for selecting this fitting range is that in this range, the hardening tendency of the true stress-true strain curve was stabilised. In the fitting process, the optimum variables of all hardening models were calculated. Once these variables were known, all hardening models were extended up to 100% of the plastic strain. As the employed hardening models were of different mathematical features, the stress difference among them was increasingly noticeable as the strain level increased (Figure 4). It is important to highlight that the hardening model predictions calculated in this work extend the hardening curve starting from the last value of the BNM curve (necking point). That is to say, the hardening curve introduced in the virtual simulation software was composed of experimental BNM values until the necking point, and from that point on optimum hardening model predictions were used to extend the curve.

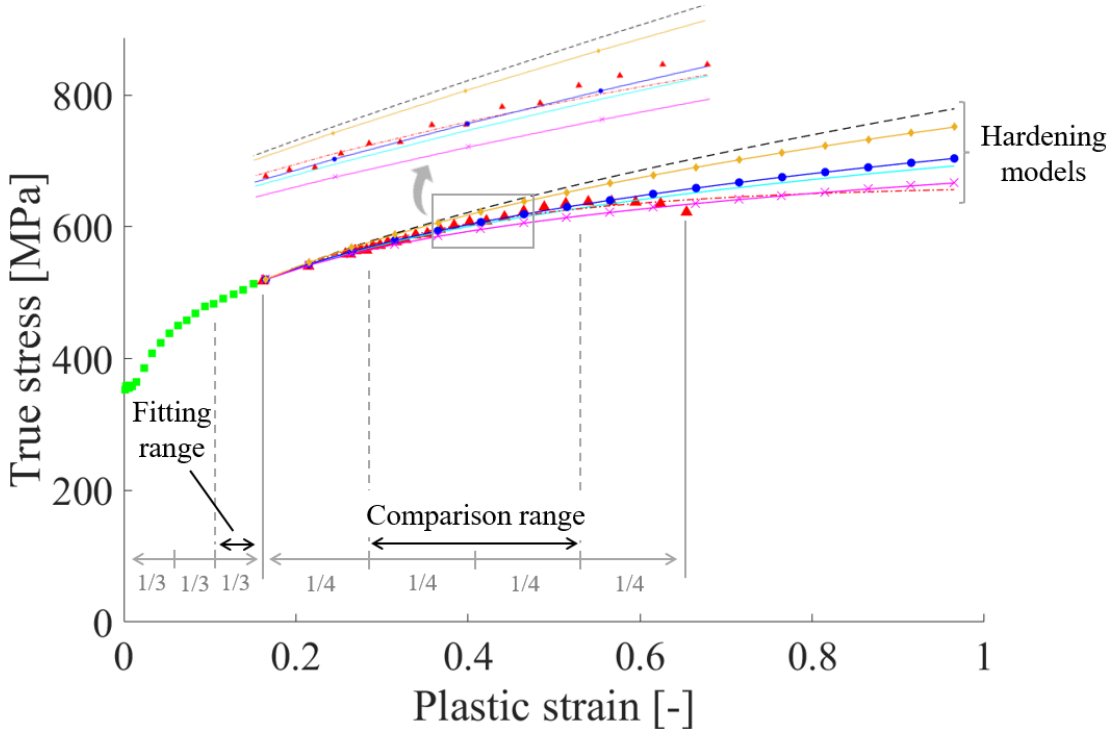

Figure 4: Fitting and comparison ranges

Secondly, to evaluate the suitability of each hardening model for representing the material hardening behaviour, errors among the experimental ANM curve and model predictions were calculated. These errors were calculated within the second and the third quarters of the ANM curve (Figure 4). The first quarter was disregarded due to the

similarity in the predictions of all the hardening models. The errors were negligible. The fourth quarter was also disregarded because the final values of a tensile test acquired by the ANM method are considered invalid due to the proximity of the specimen fracture (GOM, 2014). Thus, in the last part of the ANM curve, the homogeneity of the measured area vanishes, and the theory of the average stress-strain values is not fully accurate.

Relative errors in the comparison range among the experimental ANM data and the hardening model predictions were calculated using the following equation (1):

$$\text{error} = \frac{1}{n} \cdot \left(\sum_{1}^{n} \left| \sigma_{\text{num}_n} - \sigma_{\text{exp}_n} \right| \right), \tag{1}$$

where σ_{num} represents the stress value predicted by the hardening model, σ_{exp} represents the experimental stress value obtained by the ANM strategy and n represents the quantity of the analysed data.

Finally, taking into account the errors calculated with equation (1), a final selection of the most appropriate hardening model was made for each of the analysed material families. The most suitable hardening models were the ones with the lowest error values.

2.1 MODELS

In Table 1, the seven hardening models employed in this work (2–8) are presented. These mathematical models were utilised to extend the stress-strain curves of materials up to large strain values to then enter them in the virtual simulation software. This kind of software requires information about the stress behaviour of the processing material at all the strain stages during the metal-forming process simulation. The hardening models employed were based on diverse mathematical features, and thus were capable of describing different hardening patterns. Depending on the hardening nature of the material, some models are more suitable than others.

Table 1: Hardening models

Hardening model	Abbreviation	Formula	
Hollomon (Hollomon, 1945)	H	$\sigma(\varepsilon_{\text{p}}) = C_1 \cdot \varepsilon_{\text{p}}^{\,C_2}$	(2)
Ludwik (Ludwik, 1909)	L	$\sigma(\varepsilon_{\text{p}}) = \sigma_0 + C_1 \cdot \varepsilon_{\text{p}}^{\,C_2}$	(3)
Swift (Swift, 1952)	S	$\sigma(\varepsilon_{\text{p}}) = C_1 \cdot (\varepsilon_0 + \varepsilon_{\text{p}})^{C_2}$	(4)

Voce (Voce, 1948)	V	$\sigma(\varepsilon_p) = C_1 + (\sigma_0 - C_1) \cdot \exp(-C_2 \cdot \varepsilon_p)$	(5)
Hockett/Sherby (Hockett and Sherby, 1975)	HS	$\sigma(\varepsilon_p) = C_1 - (C_1 - \sigma_0) \cdot \exp(-C_2 \cdot \varepsilon_p^{C_3})$	(6)
Gosh (Ghosh, 1977)	G	$\sigma(\varepsilon_p) = C_1 \cdot (\varepsilon_0 + \varepsilon_p)^{C_2} - C_3$	(7)
Swift-Hockett/Sherby (Kaps et al., 1999)	SHS	$\sigma(\varepsilon_p) = C_1 \cdot (\varepsilon_0 + \varepsilon_p)^{C_2} + C_3 \cdot \exp(-C_4 \cdot \varepsilon_p^{C_5})$	(8)

2.2 MATERIALS

In this work, a wide variety of materials were analysed, such as mild steels, dual-phase steels, third-generation steels, martensitic steels and titanium alloys, representing a broad range of materials currently employed in the industrial environment. Some of the materials were analysed at various thicknesses; however, as the results of the fittings did not differ from thickness to thickness, the final model calculations were carried out taking into account only one thickness per material. The flow curves of the materials that were analysed can be seen in Figure 1.

The analysed materials were classified into six different material families. The first family analysed was the dual-phase steel family. Materials belonging to this group were the DP780, the DP980, the VOESTALPINE 1880 and the NIPPON DP1310. These steels are new AHSS and were developed mainly for the automotive industry. Other analysed steels included the conventional DX54D and DX56D steels, which were grouped within the mild steel family. These steels offer high elongation levels, low strength properties and are especially utilised for deep and extra-deep drawing operations.

Another material family analysed was the transformation-induced plasticity (TRIP) steel family. Two steels were analysed in this group, the TRIP700 and the new NIPPON TRIP1180. Steels belonging to this family provide high strength together with high ductility levels. The MS1200 steel of martensitic steel family was also studied. This steel is primarily utilised in roll-formed and tubular applications in which high strength is needed. Steels in this family offer high strength properties but a very limited formability. The last of the analysed steel families was the third-generation steel family. This UHSS group was developed to provide an additional weight reduction in cars by improving the mechanical properties of AHSS while maintaining the formability. This steel family was represented by the new FORTIFORM 1180.

In addition to steel families, titanium Grade 2 of the titanium-based material family was examined. This unalloyed titanium grade is employed in applications such as airframes, aircraft engines or marine chemical parts, and it is cold formable. Table 2 summarises the mechanical properties and thicknesses of all the studied materials classified in the above material groups.

Table 2: Mechanical properties of the analysed materials

Group	Material	t [mm]	$Rp_{0,2}$ [MPa]	Rm (True) [MPa]	Rm (Eng.) [MPa]	ε_0 [%]	$\varepsilon_{necking}$ [%]
Dual-phase	DP780	1.3	490	885	786	0.44	12.60
	DP980	1.5	739	1015	962	0.56	5.47
	VOESTALPINE1180	1.2	982	1348	1212	0.8	11.22
	NIPPON DP1310	1.6	1132	1402	1331	0.83	5.32
Mild	DX54D	0.6	153	395	310	0.3	27.72
	DX56D	0.77	161	384	300	0.29	27.76
Transformation-induced plasticity	TRIP700	1.5	513	925	726	0.47	27.35
	NIPPON TRIP1180	1	970	1363	1247	0.78	9.34
Martensitic	MS1200	1.5	1349	1370	1354	0.85	1.19
3rd-generation	FORTIFORM 1180	1.2	1071	1363	1247	0.8	9.27
Ti-based	Ti G2	1.55	315	509	442	0.44	15.18

3. RESULTS AND DISCUSSION

Once the values were calculated, the final selection of the best hardening model for each material family was carried out. The most appropriate hardening model for each material family was the one whose average error value, taking into account all the materials in the family, was the lowest. Therefore, in some materials, the selected hardening model was not the one with the lowest individual error value but that with the lowest average error value, considering all the materials in the group.

In Table 3, the results of the dual-phase steels are shown. In this case, four materials were analysed: DP780, DP980 and the new VOESTALPINE DP1180 and NIPPON DP1310. The *Error* column, based on equation (1),

shows the error value of each hardening model, while the values in the *Variables* column are the constants which constitute the hardening model expression for each material.

Table 3: Error results and fitted hardening model variables of the analysed dual phase steels

Material	Hardening model	Error	Variables				
			C1	C2	C3	C4	C5
DP780	H	13.43	1145	0.122			
	L	14.73	715	0.284			
	S	13.74	1153	0.128			
	V	4.07	913	21.8			
	HS	8.04	949	9.22	0.736		
	G	13.08	3000	0.04	1875		
	SHS	13.74	1153	0.128	-5e-10	0.489	14.2
DP980	H	12.49	1245	0.067			
	L	6.87	598	0.255			
	S	5.58	1270	0.076			
	V	95.39	1033	57.5			
	HS	68.24	1063	14.4	0.668		
	G	9.20	3000	0.029	1750		
	SHS	5.58	1270	0.076	-1e-10	-1.47	6.7
VOEST. 1180 DP	H	3.65	1668	0.094			
	L	13.90	860	0.433			
	S	2.18	1692	0.104			
	V	36.47	1396	19			
	HS	11.02	2800	0.586	0.473		
	G	2.18	1692	0.104	4e-10		
	SHS	2.18	1691	0.104	0.823	0.303	11.2
NIPPON 1310 DP	H	25.75	1614	0.044			
	L	31.23	566	0.249			
	S	29.70	1651	0.054			
	V	10.00	1420	66.5			
	HS	30.49	2800	0.398	0.27		
	G	29.14	2784	0.03	1143		
	SHS	29.71	1651	0.054	0.558	0.428	9.77

Taking into account the relative error of each hardening model, it was concluded that the *Swift* model best fits the four analysed materials. The objective of these fittings was to obtain the optimum parameters to extend the

hardening behaviours of these materials beyond the necking. The hardening predictions of the *Swift* model are shown in Figure 5.

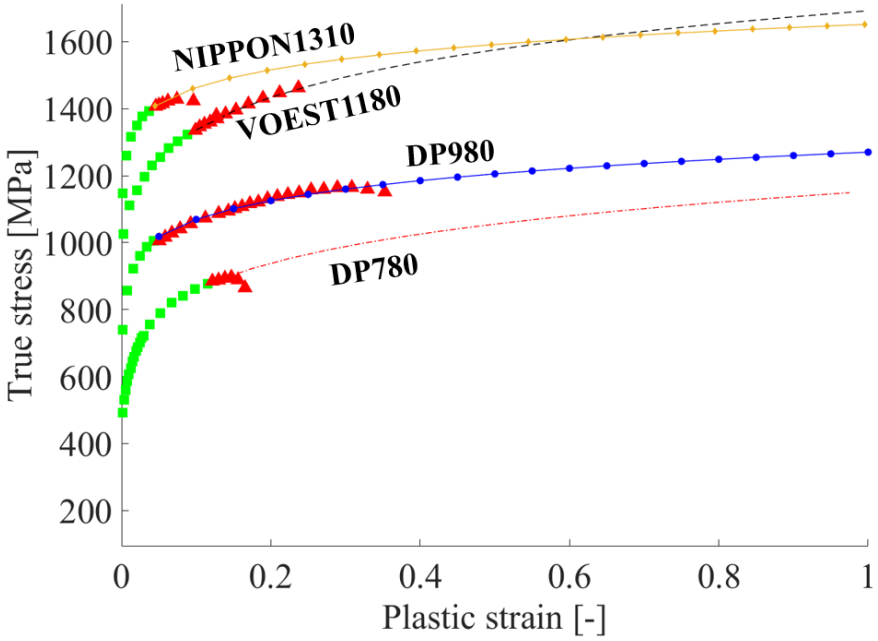

Figure 5: *Swift* hardening model prediction for the analysed dual-phase steels

Values of the calculated results for the mild steel group are shown in Table 4. In this material family, two materials were analysed: DX54D and DX56D.

Table 4: Error results and fitted hardening model variables of the analysed mild steels

Material	Hardening model	Error	Variables				
			C1	C2	C3	C4	C5
DX54D	H	6.62	507	0.201			
	L	7.30	366	0.344			
	S	6.68	507	0.204			
	V	2.81	417	8.23			
	HS	4.09	444	4.55	0.771		
	G	5.89	3000	0.027	2509		
	SHS	6.68	507	0.204	0.823	0.311	10.47
DX56D	H	2.89	504	0.219			
	L	5.00	362	0.397			
	S	2.68	504	0.222			
	V	36.66	413	7.23			

HS	2.42	992	0.548	0.457		
G	2.68	504	0.222	-4e-10		
SHS	2.64	502	0.223	2.12	-0.394	6.67

Based on the average relative error of each hardening model, it was concluded that the *Hockett/Sherby* model was that which best fit the two analysed materials. The hardening predictions of this model are shown in Figure 6.

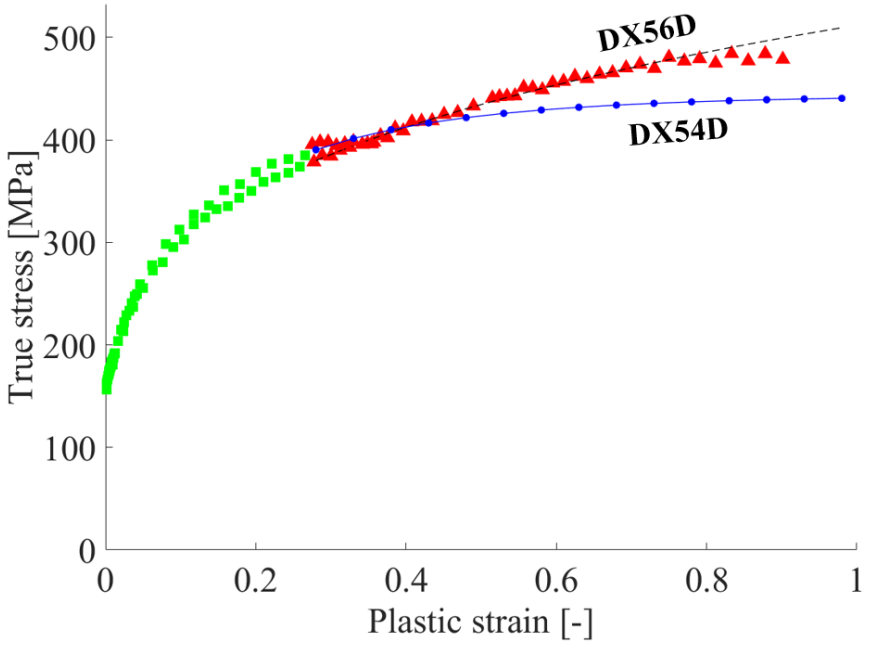

Figure 6: *Hockett/Sherby* hardening model prediction for the analysed mild steels

The results for the transformation-induced plasticity steels are shown in Table 5. Two materials were analysed: TRIP700 and the new NIPPON TRIP1180.

Table 5: Error results and fitted hardening model variables of the analysed TRIP steels

Material	**Hardening model**	**Error**	**Variables**				
			C1	**C2**	**C3**	**C4**	**C5**
TRIP700	H	1.68	1228	0.216			
	L	16.45	809	0.519			
	S	1.94	1231	0.221			
	V	29.42	1048	5.4			
	HS	12.74	2800	0.416	0.568		
	G	1.94	1231	0.221	-5e-11		

	SHS	18.76	807	0.552	531	-286	12974
NIPPON TRIP 1180	H	10.34	1687	0.086			
	L	9.63	840	0.354			
	S	6.29	1714	0.096			
	V	72.76	1405	26.2			
	HS	3.95	1989	1.31	0.437		
	G	6.29	1714	0.096	-1.4e-5		
	SHS	6.29	1713	0.096	0.971	0.357	14.4

In this case, the most suitable hardening model was determined to be the *Ghosh* model based on the average error value. Figure 7 shows the prediction of the optimum hardening model for this material family.

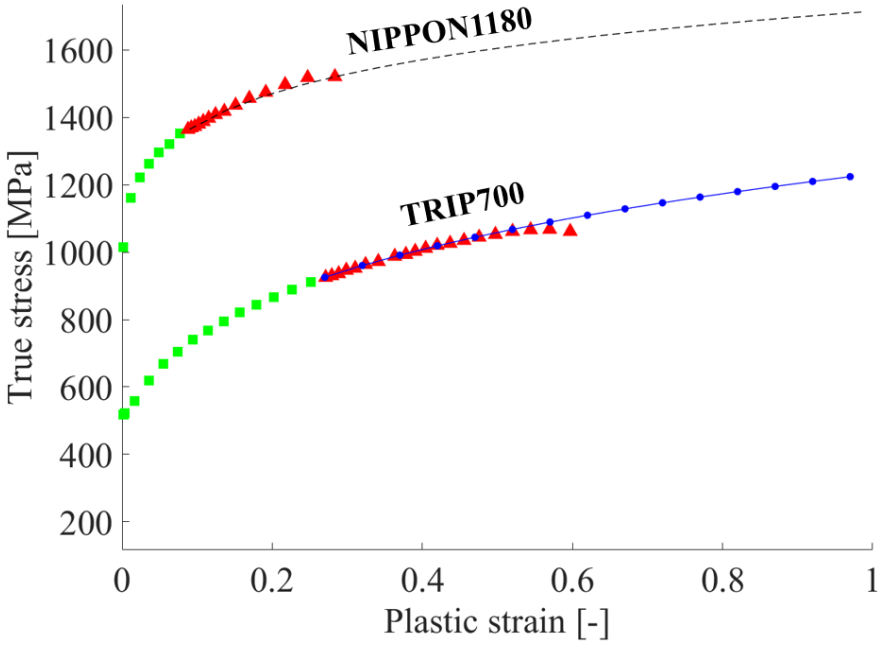

Figure 7: *Ghosh* hardening model prediction for the analysed transformation-induced plasticity steels

The values for the martensitic steel are shown in Table 6. In the case of this material family a single material was analysed: MS1200.

Table 6: Error results and fitted hardening model variables of the analysed martensitic steel

Material	**Hardening model**	**Error**	**Variables**				
			C1	**C2**	**C3**	**C4**	**C5**
MS1200	H	74.12	1416	0.006			
	L	176.84	2529	0.974			

S	26.59	1523	0.024			
V	23.02	1519	19.1			
HS	20.16	1514	19.9	1		
G	26.74	1626	0.022	104		
SHS	26.59	1522	0.024	0.557	0.067	17.7

In this case, the *Hockett/Sherby* model was identified as the most suitable hardening model. Figure 8 shows the prediction of the optimum hardening model for this material.

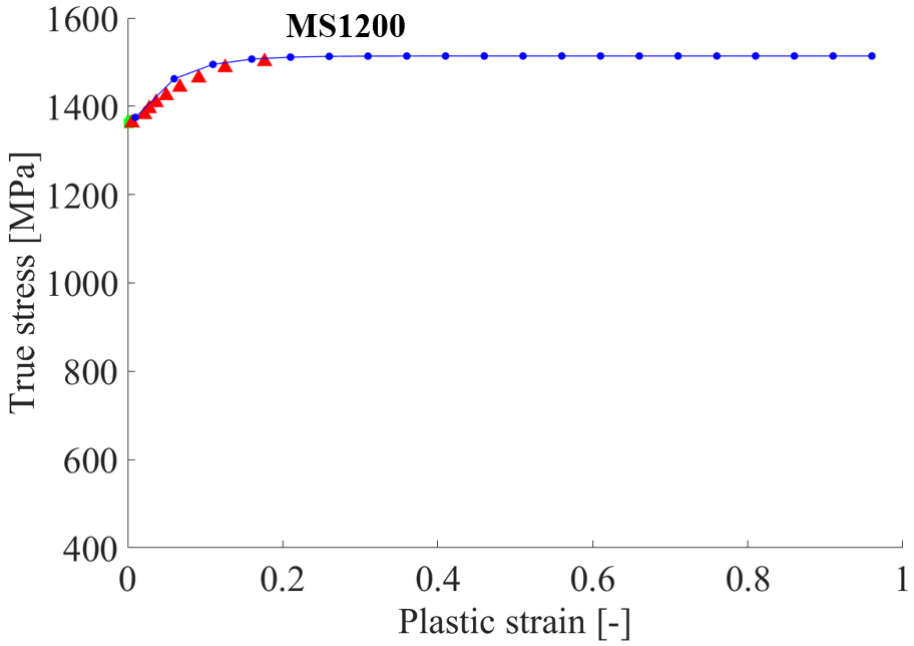

Figure 8: *Hockett/Sherby* hardening model prediction for the analysed martensitic steel

For the last of the steel families, the results for a third-generation steel are shown in Table 7. A single material was analysed: the new FORTIFORM 1180.

Table 7: Error results and fitted hardening model variables of the analysed third generation steel

Material	**Hardening model**	**Error**	**Variables**				
			C1	**C2**	**C3**	**C4**	**C5**
FORTIF. 1180	H	3.20	1651	0.078			
	L	11.25	756	0.394			
	S	1.56	1674	0.087			
	V	38.08	1406	23.5			
	HS	5.92	1548	4.2	0.513		

	G	2.17	3000	0.043	1344		
	SHS	1.56	1674	0.087	0.726	0.285	15

As for the dual-phase family, the most suitable hardening model was the *Swift* model. Figure 9 shows the prediction of the optimum hardening model for this material.

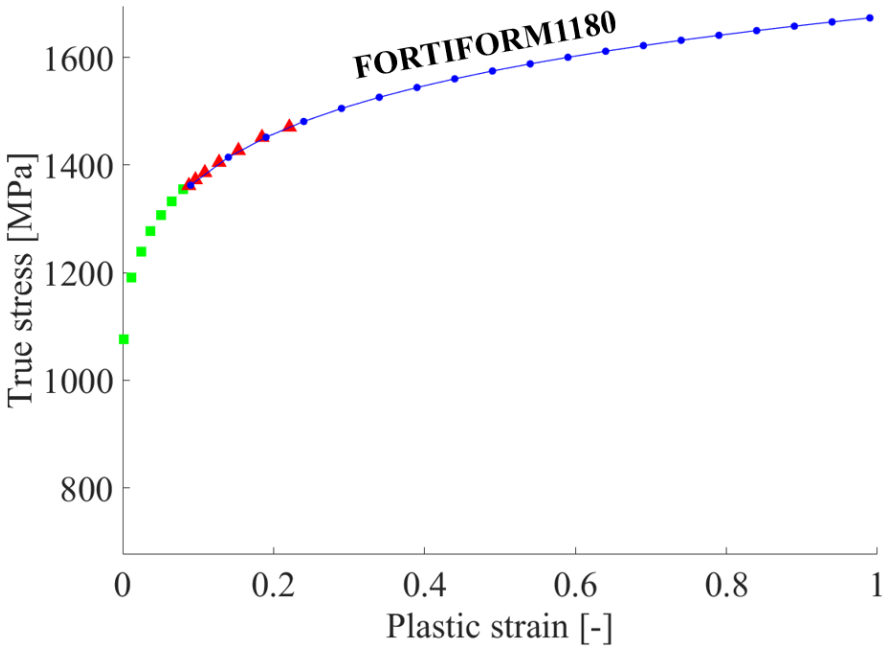

Figure 9: *Swift* hardening model prediction for the analysed third generation steel

Finally, the results for titanium are shown in Table 8. Once again, a single material was analysed: Ti G2.

Table 8: Error results and fitted hardening model variables of the analysed grade 2 titanium alloy

Material	**Hardening model**	**Error**	**Variables**				
			C1	**C2**	**C3**	**C4**	**C5**
Ti G2	H	9.91	643	0.123			
	L	1.52	367	0.344			
	S	8.90	646	0.128			
	V	46.05	529	15.4			
	HS	2.02	2800	0.158	0.357		
	G	8.90	646	0.128	-0.001		
	SHS	8.83	642	0.129	4.32	-1.07	5.39

In this case, the most suitable hardening model was determined to be the *Ludwik* model. Figure 10 shows the prediction of the optimum hardening model for this material.

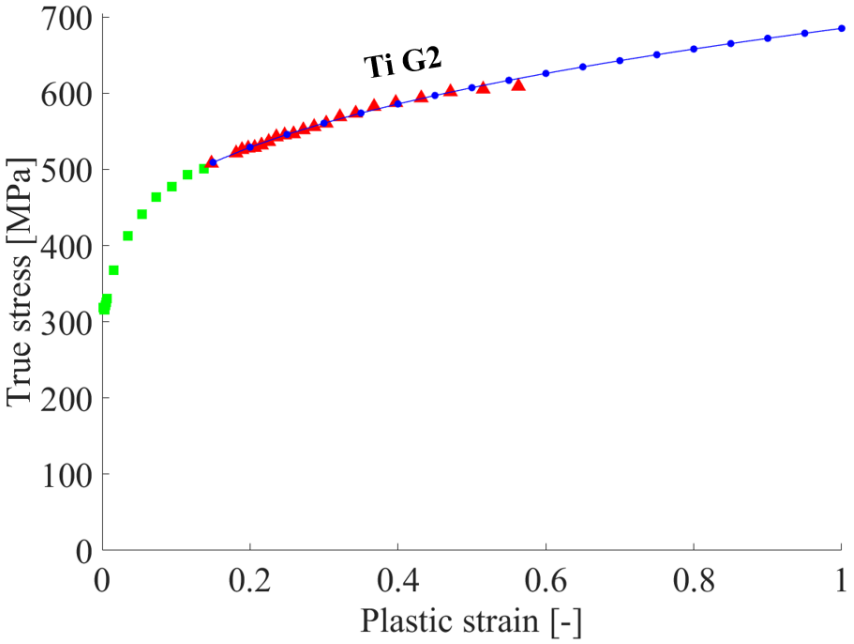

Figure 10: *Ludwik* hardening model prediction for the analysed titanium grade 2 alloy

The hardening variables presented in Table 4–Table 8 were utilised to extend the experimental curves of the materials starting from the necking point (the last value of the BNM curve). The validity of the hardening model predictions in smaller strains prior to the necking limit was not analysed.

The results presented in this section show that in some cases, such as in the TRIP steel family, two of the analysed models had the same minimum error value (*Swift* and *Ghosh*); therefore, both models can be valid. The model selected as the most suitable hardening model was the one with the minimum average error value; however, in some cases, the error difference among the models was negligible, so in such cases, more than one model could represent the hardening behaviour of the material.

Finally, a summary of the results is presented in Table 9, in which the optimum hardening model for each of the analysed material families is shown.

Table 9: Optimum hardening model for each analysed material family

Material family	**Optimum hardening model**
Dual-phase	*Swift*
Mild	*Hockett/Sherby*
Transformation-induced plasticity	*Ghosh*

Martensitic	*Hockett/Sherby*
3rd-generation	*Swift*
Ti-based	*Ludwik*

4. CONCLUSIONS

This paper aims to determine the optimum hardening model for a broad variety of material families to predict their hardening at high strain levels. The DIC technique was utilised to obtain experimental hardening data of the materials and several commonly used models were analysed to select that with the best ability to represent each hardening behaviour. The conclusions based on this procedure are as follows.

- The DIC technique is a simple method for the extension of the stress-strain curve of a wide variety of materials. Based on a conventional tensile test, by just adding external artificial vision devices, larger strains than those obtained in standard tensile tests can be achieved. However, to support this statement and obtain experimental values at higher strain levels, the performance of tests such as the shear test or the bulge test would be enriching.

- The ANM curve extension varies depending on the material stretching capacity. In low-strength steels, greater experimental extensions are obtained in comparison to high-strength steels. This effect could be due to the necking to fracture behaviour of each material.

- In material families in which just one material was analysed, further analysis of more materials needs to be carried out to determine the appropriateness of the selected hardening model.

- Aspects, such as temperature and strain rate, have a significant effect in industrial sheet metal forming processes. Therefore, further research should be undertaken to investigate their influence on the hardening behaviour of the analysed materials.

5. ACKNOWLEDGEMENTS

The work presented in this article was carried out in cooperation with MATRICI S. Coop. It was financially supported by the project HRD (High Reliability Dies) project, under the program RETOS, reference number RTC-2015-3643-4, and was financed by the Spanish government through the Ministry of Economy and Competitiveness.

6. REFERENCES

Askari-paykani, M., Shahverdi, H.R., Miresmaeili, R., 2016. Journal of Materials Processing Technology First and third generations of advanced high-strength steels in a FeCrNiBSi system. J. Mater. Process. Tech. 238, 383–394. doi:10.1016/j.jmatprotec.2016.07.043

Avril, S., Bonnet, M., Bretelle, A.S., Grediac, M., Hild, F., Ienny, P., Latourte, F., Lemosse, D., Pagano, S., Pagnacco, E., 2008. Overview of identification methods of mechanical parameters based on full-field measurements.

Butuc, M.C., Teodosiu, C., Barlat, F., Gracio, J.J., 2011. Analysis of sheet metal formability through isotropic and kinematic hardening models. Eur. J. Mech. - A/Solids 30, 532–546. doi:10.1016/j.euromechsol.2011.03.005

Coppieters, S., Cooreman, S., Sol, H., Van Houtte, P., Debruyne, D., 2011. Identification of the post-necking hardening behaviour of sheet metal by comparison of the internal and external work in the necking zone. J. Mater. Process. Technol. 211, 545–552. doi:10.1016/j.jmatprotec.2010.11.015

Coppieters, S., Kuwabara, T., 2014. Identification of Post-Necking Hardening Phenomena in Ductile Sheet Metal. Exp. Mech. 54, 1355–1371. doi:10.1007/s11340-014-9900-4

Eller, T.K., Greve, L., Andres, M., Medricky, M., Meinders, V.T., van den Boogaard, A.H., 2016. Determination of strain hardening parameters of tailor hardened boron steel up to high strains using inverse FEM optimization and strain field matching. J. Mater. Process. Technol. 228, 43–58. doi:10.1016/j.jmatprotec.2015.09.036

Gerbig, D., Bower, A., Savic, V., Hector, L.G., 2016. Coupling digital image correlation and finite element analysis to determine constitutive parameters in necking tensile specimens. Int. J. Solids Struct. 97_98, 496–509. doi:10.1016/j.ijsolstr.2016.06.038

Ghosh, A.., 1977. Tensile instability and necking in materials with strain hardening and strain-rate hardening. Acta Metall. 25, 1413–1424. doi:10.1016/0001-6160(77)90072-4

Gil, I., Mendiguren, J., Galdos, L., Mugarra, E., Saenz de Argandoña, E., 2016. Influence of the pressure dependent coefficient of friction on deep drawing springback predictions. Tribol. Int. 103, 266–273. doi:10.1016/j.triboint.2016.07.004

GOM, 2016. ARAMIS [WWW Document]. URL http://www.gom.com/metrology-systems/aramis.html (accessed 2.14.17).

GOM, 2014. Optical Measuring Techniques ARAMIS user manual - Tensile test evaluation.

González Palencia, J.C., Furubayashi, T., Nakata, T., 2012. Energy use and CO2 emissions reduction potential in passenger car fleet using zero emission vehicles and lightweight materials. Energy 48, 548–565. doi:10.1016/j.energy.2012.09.041

Grédiac, M., Pierron, F., 2006. Applying the Virtual Fields Method to the identification of elasto-plastic constitutive parameters. Int. J. Plast. 22, 602–627. doi:10.1016/j.ijplas.2005.04.007

Hockett, J.E., Sherby, O.D., 1975. Large strain deformation of polycrystalline metals at low homologous temperatures. J. Mech. Phys. Solids 23, 87–98. doi:10.1016/0022-5096(75)90018-6

Hollomon, J.H., 1945. Tensile deformation. Trans. Metall. Soc. AIME 162, 268–290.

Holmberg, S., Enquist, B., Thilderkvist, P., 2004. Evaluation of sheet metal formability by tensile tests. J. Mater. Process. Technol. 145, 72–83. doi:10.1016/j.jmatprotec.2003.07.004

Hora, P., 2006. Advanced Constitutive Models as Precondition for an Accurate FEM-Simulation in Forming Keynote-Paper. LS-DYNA Anwenderforum 1–74.

Kaps, L., Lipowski, H.J., Meywerk, M., Werner, H., Scholz, S.-P., 1999. Auswerteverfahren zur Weiterverarbeitung von Versuchsdaten. VDEH working group intern communication.

Kuwabara, T., 2007. Advances in experiments on metal sheets and tubes in support of constitutive modeling and forming simulations. Int. J. Plast. 23, 385–419. doi:10.1016/j.ijplas.2006.06.003

Larour, P., 2010. Strain rate sensitivity of automotive sheet steels: influence of plastic strain, strain rate, temperature, microstructure, bake hardening and pre-strain.

Lee, J.Y., Barlat, F., Lee, M.G., 2015. Constitutive and friction modeling for accurate springback analysis of advanced high strength steel sheets. Int. J. Plast. 71, 113–135. doi:10.1016/j.ijplas.2015.04.005

Liu, W., Guines, D., Leotoing, L., Ragneau, E., 2015. Identification of sheet metal hardening for large strains with an in-plane biaxial tensile test and a dedicated cross specimen. Int. J. Mech. Sci. 101, 387–398. doi:10.1016/j.ijmecsci.2015.08.022

Ludwik, P., 1909. Elemente der Technologischen Mechanik. doi:10.1007/978-3-662-40293-1

Manopulo, N., Barlat, F., Hora, P., 2015. Isotropic to distortional hardening transition in metal plasticity. Int. J.

Solids Struct. 56, 11–19. doi:10.1016/j.ijsolstr.2014.12.015
Mendiguren, J., Cortés, F., Gómez, X., Galdos, L., 2015a. Elastic behaviour characterisation of TRIP 700 steel by means of loading–unloading tests. Mater. Sci. Eng. A 634, 147–152. doi:10.1016/j.msea.2015.03.050
Mendiguren, J., Rolfe, B., Weiss, M., 2015b. On the definition of an kinematic hardening effect graph for sheet metal forming process simulations. Int. J. Mech. Sci. 92, 109–120. doi:10.1016/j.ijmecsci.2014.12.005
Merklein, M., Biasutti, M., 2013. Development of a biaxial tensile machine for characterization of sheet metals. J. Mater. Process. Technol. 213, 939–946. doi:10.1016/j.jmatprotec.2012.12.005
Merklein, M., Lechler, J., Geiger, M., 2006. Characterisation of the Flow Properties of the Quenchenable Ultra High Strength Steel 22MnB5. CIRP Ann. - Manuf. Technol. 55, 229–232. doi:10.1016/S0007-8506(07)60404-1
Mulder, J., Vegter, H., Aretz, H., Keller, S., van den Boogaard, A.H., 2015. Accurate determination of flow curves using the bulge test with optical measuring systems. J. Mater. Process. Technol. 226, 169–187. doi:10.1016/j.jmatprotec.2015.06.034
Neto, D.M., Oliveira, M.C., Santos, A.D., Alves, J.L., Menezes, L.F., 2017. Influence of boundary conditions on the prediction of springback and wrinkling in sheet metal forming. Int. J. Mech. Sci. 122, 244–254. doi:10.1016/j.ijmecsci.2017.01.037
Nolan, D.R., McGarry, J.P., 2016. On the correct interpretation of measured force and calculation of material stress in biaxial tests. J. Mech. Behav. Biomed. Mater. 53, 187–199. doi:10.1016/j.jmbbm.2015.08.019
Oliveira, M.C., Alves, J.L., Chaparro, B.M., Menezes, L.F., 2005. Study on the influence of the work hardening models constitutive parameters identification in the springback prediction. AIP Conf. Proc. 778 A, 253–258. doi:10.1063/1.2011228
Panich, S., Suranuntchai, S., Jirathearanat, S., Uthaisangsuk, V., 2016. A hybrid method for prediction of damage initiation and fracture and its application to forming limit analysis of advanced high strength steel sheet. Eng. Fract. Mech. 166, 97–127. doi:10.1016/j.engfracmech.2016.08.025
Peng, L.F., Xu, Z.T., Fu, M.W., Lai, X.M., 2017. Forming limit of sheet metals in meso-scale plastic forming by using different failure criteria. Int. J. Mech. Sci. 120, 190–203. doi:10.1016/j.ijmecsci.2016.11.021
Processes, F., 2008. NSM Simulation and Optimization of Metal Forming Processes 1–27.
Rossi, M., Chiappini, G., Sasso, M., 2013. Characterization of aluminum alloys using a 3D full field measurement. Springer, New York, NY, pp. 17–23. doi:10.1007/978-1-4419-9796-8_4
Saboori, M., Champliaud, H., Gholipour, J., Gakwaya, A., Savoie, J., Wanjara, P., 2014. Evaluating the flow stress of aerospace alloys for tube hydroforming process by free expansion testing. Int. J. Adv. Manuf. Technol. 72, 1275–1286. doi:10.1007/s00170-014-5670-5
Silvestre, E., Mendiguren, J., Galdos, L., Sáenz De Argandoña, E., 2015. Comparison of the hardening behaviour of different steel families: From mild and stainless steel to advanced high strength steels. Int. J. Mech. Sci. 101–102, 10–20. doi:10.1016/j.ijmecsci.2015.07.013
Suttner, S., Merklein, M., 2017. A new approach for the determination of the linear elastic modulus from uniaxial tensile tests of sheet metals. J. Mater. Process. Technol. 241, 64–72. doi:10.1016/j.jmatprotec.2016.10.024
Suttner, S., Merklein, M., 2016. Experimental and numerical investigation of a strain rate controlled hydraulic bulge test of sheet metal. J. Mater. Process. Technol. 235, 121–133. doi:10.1016/j.jmatprotec.2016.04.022
Sutton, Michael , Jean-José, Orteu Schreier, A.H., 2009. Image Correlation for Shape, Motion and Deformation Measurements, Springer Science+Business Media. doi:10.1017/CBO9781107415324.004
Swift, H.W., 1952. Plastic instability under plane stress. J. Mech. Phys. Solids 1, 1–18.
Teixeira, P., Santos, A.D., Andrade Pires, F.M., César de Sá, J.M.A., 2006. Finite element prediction of ductile fracture in sheet metal forming processes. J. Mater. Process. Technol. 177, 278–281. doi:10.1016/j.jmatprotec.2006.04.059
Ul Hassan, H., Traphöner, H., Güner, A., Tekkaya, A.E., 2016. Accurate springback prediction in deep drawing using pre-strain based multiple cyclic stress-strain curves in finite element simulation. Int. J. Mech. Sci. 110, 229–241. doi:10.1016/j.ijmecsci.2016.03.014
Voce, E., 1948. The relationship between stress and strain for homogeneous deformation. J. Int. Met. 74, 537–562.
Wang, W., Zhao, Y., Wang, Z., Hua, M., Wei, X., 2016. A study on variable friction model in sheet metal forming with advanced high strength steels. Tribol. Int. 93, 17–28. doi:10.1016/j.triboint.2015.09.011
Weiss, M., Kupke, A., Manach, P.Y., Galdos, L., Hodgson, P.D., 2015. On the Bauschinger effect in dual phase steel at high levels of strain. Mater. Sci. Eng. A 643, 127–136. doi:10.1016/j.msea.2015.07.037
Yin, Q., Soyarslan, C., Isik, K., Tekkaya, A.E., 2015. A grooved in-plane torsion test for the investigation of shear fracture in sheet materials. Int. J. Solids Struct. 66, 121–132. doi:http://dx.doi.org/10.1016/j.ijsolstr.2015.03.032

Yin, Q., Zillmann, B., Suttner, S., Gerstein, G., Biasutti, M., Tekkaya, A.E., Wagner, M.F.X., Merklein, M., Schaper, M., Halle, T., Brosius, A., 2014. An experimental and numerical investigation of different shear test configurations for sheet metal characterization. Int. J. Solids Struct. 51, 1066–1074. doi:10.1016/j.ijsolstr.2013.12.006

Yu, H., Chen, S.J., 2017. A mixed hardening model combined with the transformation-induced plasticity effect. J. Manuf. Process. doi:10.1016/j.jmapro.2016.12.012

Zhang, J., Di, H., Deng, Y., Misra, R.D.K., 2015. Effect of martensite morphology and volume fraction on strain hardening and fracture behavior of martensite–ferrite dual phase steel. Mater. Sci. Eng. A 627, 230–240. doi:10.1016/j.msea.2015.01.006

Zillmann, B., Wagner, M.F.X., Schmaltz, S., Schmidl, E., Lampke, T., Willner, K., Halle, T., 2014. In-plane biaxial compression and tension testing of thin sheet materials. Int. J. Solids Struct. 66, 111–120. doi:10.1016/j.ijsolstr.2015.03.031